Soft Matter

Controlling Shear Jamming in Dense Suspensions via the Particle Aspect Ratio

Journal:	*Soft Matter*
Manuscript ID	SM-COM-02-2019-000335.R1
Article Type:	Communication
Date Submitted by the Author:	01-Apr-2019
Complete List of Authors:	James, Nicole; The University of Chicago, Chemistry Department; The University of Chicago, James Franck Institute Xue, Huayue; The University of Chicago, Physics; The University of Chicago, James Franck Institute Goyal, Medha; The University of Chicago, Physics; The University of Chicago, James Franck Institute Jaeger, Heinrich; University of Chicago, Physics/JFI

Soft Matter

ARTICLE TYPE

Cite this: DOI: 10.1039/xxxxxxxxxx

Controlling Shear Jamming in Dense Suspensions via the Particle Aspect Ratio

Nicole M. James,[a†] Huayue Xue,[b†], Medha Goyal,[b†] and Heinrich M. Jaeger[b†*]

Received Date
Accepted Date

DOI: 10.1039/xxxxxxxxxx

www.rsc.org/journalname

Dense suspensions of particles in a liquid exhibit rich, non-Newtonian behaviors such as shear thickening (ST) and shear jamming (SJ). ST has been widely studied and is known to be enhanced by increasing the particles' frictional interactions and also by making their shape more anisotropic. SJ however has only recently been understood to be a distinct phenomenon and, while the role of interparticle friction has been investigated, the role of particle anisotropy in controlling the SJ regime remained unknown. To address this we here synthesize silica particles for use in water/glycerol suspensions. This pairing of hydrogen-bonding particle surfaces and suspension solvent has been shown to elicit SJ with spherical particles. We then vary particle aspect ratio from Γ=1 (spheres) to Γ=11 (slender rods), and perform rheological measurements to determine the effect of particle anisotropy on the onset of shear jamming. We also show that the effect on the precursor to SJ, discontinuous shear thickening (DST), is consistent with prior work. We find that increasing aspect ratio significantly reduces ϕ_m, the minimum particle packing fraction at which SJ can be observed, to values as low $\phi_m = 33\%$ for Γ=11. The ability to fix the properties of the solvated particle surfaces, and thus the particle interactions at contact, while varying shape anisotropy, yields fundamental insights about the SJ capabilities of suspensions and provides a framework to rationally design and tune these behaviors.

Dense particulate suspensions often display a variety of non-Newtonian flow properties, including shear thinning, shear thickening, and reversible, shear-induced solidification called shear jamming.[1,2] Discontinuous shear thickening (DST), where a suspension experiences a discontinuous jump in viscosity at a critical shear rate, has been studied widely.[3–7] Recently it has been understood to depend heavily on interparticle friction.[8–13] Shear jamming (SJ) is a phenomenon where a suspension is fluid-like at low stresses and jams into a solid-like state at high shear. This shear-induced solidification occurs at particle concentrations ϕ below the traditional, frictionless jamming packing fraction ϕ_0 and has often been conflated with DST which, however, remains a flowing state. Furthermore, unlike shear-induced aggregation,[14] the stress dependence of the particle interactions makes shear jamming reversible:[15,16] when the applied stress is removed, the suspension relaxes back to the fluid state.

Models and simulations[17–20] have provided a stress-dependent mechanism in which the highly viscous, yet still fluid DST state can be viewed as a precursor to the solid-like SJ state. At low applied shear, most particles in the suspension are lubricated by solvent layers, thus only weak thickening is observed. In this low-shear limit, as more particles are added, the frictionless jamming packing fraction ϕ_0 governs the onset of rigidity. As the applied shear is increased, a fraction of particles are forced into close proximity, such that the lubrication layer ruptures or is reduced to molecular length-scales, at which point the continuum models describing lubrication break down. As a result, particles are effectively in direct contact and interact frictionally. In the presence of such frictional interactions, DST occurs readily over a range for packing fractions ϕ below ϕ_0.[11–13] For sufficiently strong frictional interactions, further increase in the applied shear stress can then transition the suspension from DST into the SJ regime.

While DST has been heavily studied,[4–7] how parameters such as particle shape effect the SJ state has remained largely unexplored. In this work, we map out the rheology of suspensions as the SJ state is approached and employ the Wyart-Cates model[17] to generate state diagrams that delineate DST and SJ regimes as a function of packing density and applied shear stress for different particle aspect ratios.

In the Wyart-Cates model, SJ can be characterized by three parameters: the minimum packing fraction required for SJ, ϕ_m, the frictionless jamming packing fraction, ϕ_0, (above which the sus-

[a] Chemistry Department, The University of Chicago, Chicago, IL, USA
[b] Physics Department, The University of Chicago, Chicago, IL, USA
† James Franck Institute, The University of Chicago, Chicago, IL, USA
* Corresponding Author: h-jaeger@uchicago.edu

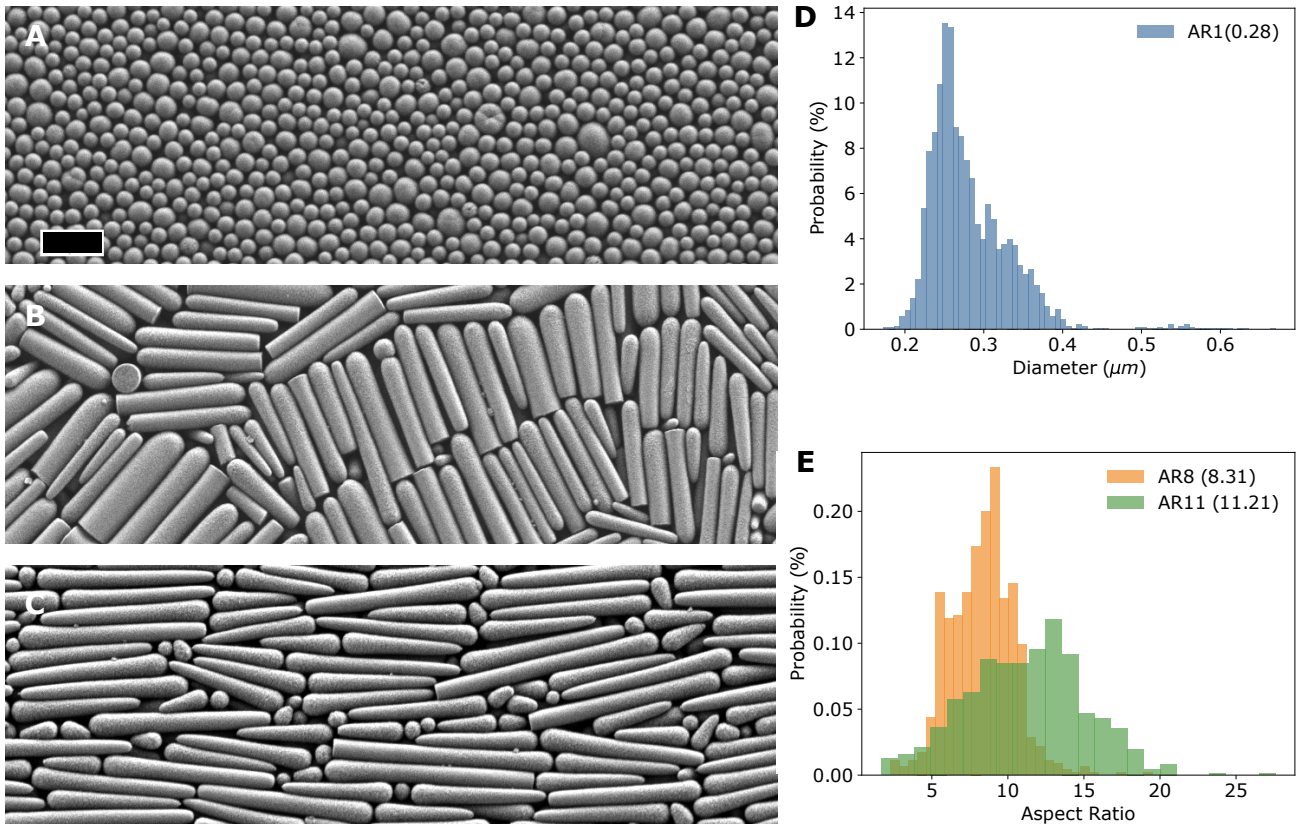

Fig. 1 SEM images and characterization for AR1, AR8 and AR11 particle systems. A. AR1 spheres (scale bar indicates 1 μm), B. AR8 rods, and C. AR11 rods. The scale bar in A. applies to subplots A-C. D. Diameter distribution for AR1 spheres. E. Aspect ratio distribution for AR8 rods and AR11 rods. The mean aspect ratio for each system is stated in parentheses.

pension is not fluid-like even at low shear), and a critical shear stress that describes the breakdown of lubrication barriers between particles, τ^*.

It is significant to note that in many systems that show robust DST, such as glass in oil,[1,21] SJ is not experimentally resolved. To elicit SJ on experimentally-accessible ϕ and τ ranges, we build upon our prior work[21] which shows that designing particle surfaces and suspending solvents to facilitate interparticle hydrogen bonding can elicit shear jamming. This work directly connected interparticle hydrogen bonding ability with an enhancement of friction that results in SJ at lower ϕ and τ. Thus for our suspensions we facilitate interparticle hydrogen bonding by using silica particles with silanol surface groups, and a polar protic solvent (water/glycerol with 15mM NaCl).

Of particular interest is the range between ϕ_m and ϕ_0. A suspension that is fluid-like at rest or low applied shear, *i.e.*, has a packing fraction $\phi < \phi_0$, can be sheared into a jammed state as long as $\phi > \phi_m$, provided the shear stresses necessary are achievable. In other words, shear jamming can be observed for any ϕ such that $\phi_0 > \phi > \phi_m$. Here we explore the extent to which the onset of experimentally-accessible jamming depends on particle shape by monitoring how the key parameters ϕ_0, ϕ_m, and τ^* vary with increasing particle aspect ratio.

On geometric grounds, we can expect that increasing the particles' aspect ratio by elongating them into rods will increase the number of contacts with neighboring particles and therefore generally enhance the ability to jam, *i.e.* reduce ϕ_0.[22] This is borne out by prior work on rod-shaped colloids[23] and dry granular materials,[24] which investigated the limit of low applied stress up to yielding or the shear thinning regime just beyond yielding. Work on suspensions of rod-like particles or fibers has also shown strong aspect ratio dependence on ϕ_0.[25] In their sheared state, however, rod-like particles will tend to align and *a priori* it is not clear whether shear jamming will be enhanced or diminished as particle aspect ratio increases. There are many examples of fiber composites that show thinning-dominated behavior.[26] Similarly, much is known about the gelation behavior of rod-like liquid crystals[27,28] and colloidal rod suspensions.[29] In suspensions where shear thickening was observed, increasing aspect ratio has been found to lower the minimum particle concentration for DST.[30–32] Still, as far as control over the shear jamming regime is concerned, the role of particle shape in tuning the shear jamming propensity (*i.e.* via ϕ_0, ϕ_m, and τ^*) has not been investigated in either simulations or experiments.

Here we report on experiments that aim to isolate the effect of particle shape anisotropy. We employ an emulsion-based synthesis of silica rods.[33] This synthesis results in bullet-shaped rods of ~250 nm diameter and controllable length. In aqueous solvents the silanol (Si-OH) surface groups enable particle-particle hydrogen bonding analogous to that we used previously to design SJ

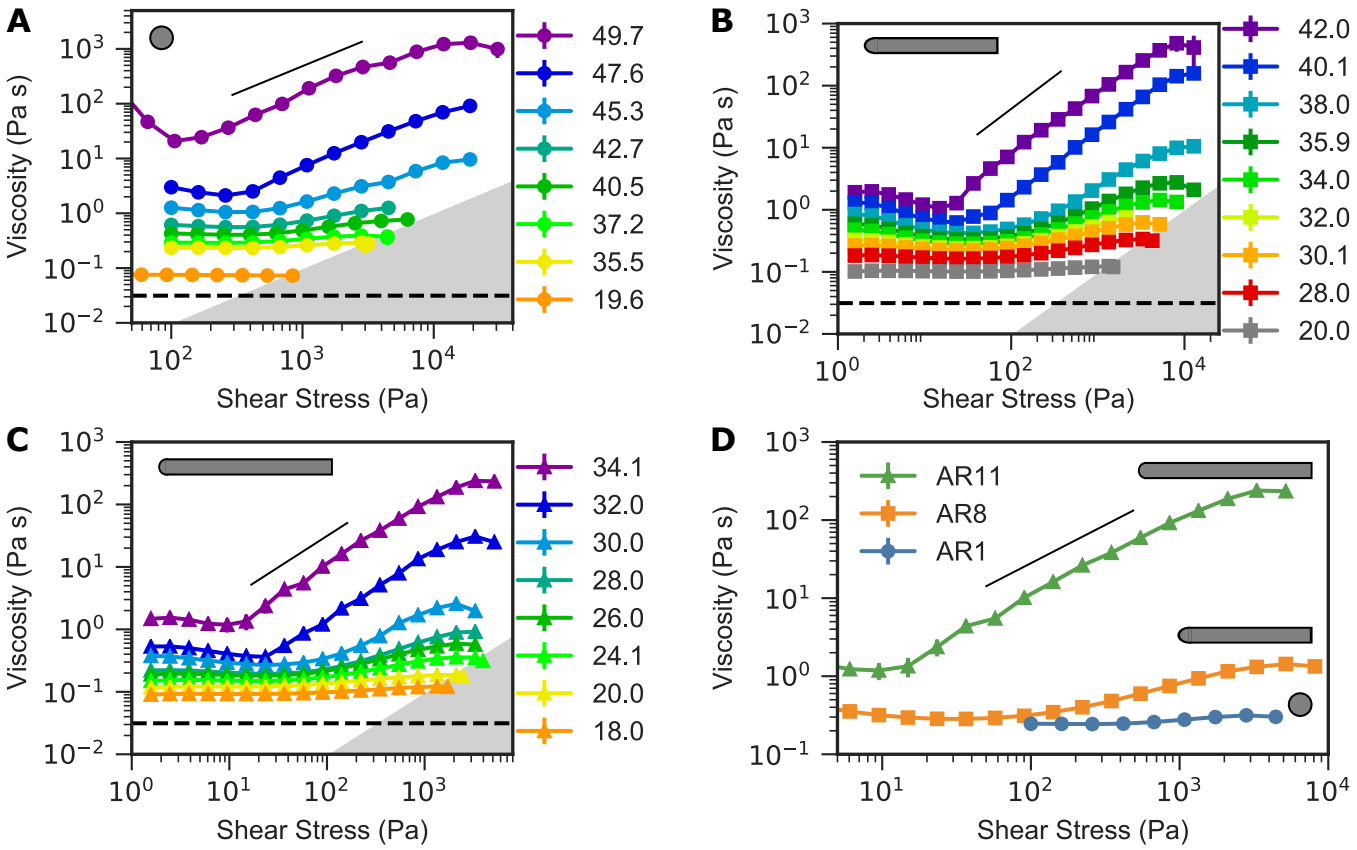

Fig. 2 Rheological flow curves for A. spheres (AR1), B. aspect ratio 8 rods (AR8), and C. aspect ratio 11 rods (AR11), at various packing fractions ϕ (%) in 70% aqueous glycerol (v/v) with 15 mM NaCl. The dashed black line indicates the suspending solvent viscosity. Solid black lines indicate a slope of 1. Gray shaded regions indicate the rheometer's rate limit. Gray icons indicate the relative difference in aspect ratio (to scale) among the systems. D. Comparison of flow curves at ϕ=34.1 $\pm$ 0.1%, highlighting the enhancement of shear thickening with increasing aspect ratio.

into model systems.[21] Particle sizes and shapes are characterized by scanning electron microscopy and image analysis. We discuss results for three characteristic systems, each with a different aspect ratio Γ (length-to-diameter): $\Gamma \approx 1$ spheres (AR1), $\Gamma \approx 8$ rods of average length 2.0 μm (AR8), and $\Gamma \approx 11$ rods of average length 2.8 μm (AR11), shown in Figure 1. Above an aspect ratio of roughly 11, this synthesis produces irregularly shaped or wavey rods.[33]

We perform stress-controlled rheological measurements on suspensions of these particles. Increasing and decreasing stress ramps were used to determine shear protocols: the establishment of a steady state was determined by the quantitative agreement of both the increasing and decreasing stress ramps. In all cases, the suspending solvent was 70% glycerol in water (v/v) with 15 mM NaCl. This solvent was selected to mediate interparticle hydrogen bonding such that the suspension shear jams. The particular glycerol and NaCl concentrations were selected to ensure the flow curves could be well resolved within the rheometer rate limit, indicated by the gray region in the lower-right of each plot in Figure 2. The AR1 system of spheres (Fig. 2a) shows mild shear thickening at $\phi = 35.5\%$ and strong, discontinuous shear thickening (DST) at $\phi = 47.6\%$. Note that a slope of 1 on log-log plots of viscosity versus stress (indicated by the solid black line) as in Fig. 2 implies a vertical, discontinuous jump if the same data are plotted versus shear rate. Concentrated packing fractions approaching $\phi = 50\%$ can be prepared and remain fluid-like. In contrast, the AR8 system (Fig. 2b) exhibits mild shear thickening as early as $\phi = 28.0\%$, and strong DST that spans over two orders of magnitude in viscosity, at only $\phi = 40.1\%$. Following this trend, the AR11 system (Fig. 2c) shows mild shear thickening at $\phi = 18.0\%$, and DST at only $\phi = 30.0\%$. To highlight the significance of this, DST with spheres typically requires packing fractions in excess of $\phi = 50\%$.

Figure 2d compares the three systems at $\phi = 34.1 \pm 0.1\%$. While the AR1 system only very slightly shear thickens, the AR11 system already shows DST. The drastic enhancement of thickening behavior with aspect ratio at a given packing fraction is in agreement with prior studies.[30–32] Here we analyze these flow curves in order to describe the shear jamming characteristics as a function of aspect ratio. The data show that the viscosity is growing rapidly as ϕ increases (see ESI Figure S1), approaching some jamming point ϕ_J, consistent with a Krieger-Dougherty-type relation[34]:

$$\eta_r = (1 - \frac{\phi}{\phi_J})^{-\beta}, \quad (1)$$

where η_r is the suspension viscosity rescaled by the suspending solvent's viscosity, ϕ_J is the jamming packing fraction.

To connect this steady state, flowing data with the solid-like

shear jammed state, we follow prior work[17,18,20] which notes that, since η_r is a function of τ, the divergence of η_r, and thus the jamming point ϕ_J, is τ-dependent. Thus using these models we define two jamming points of interest: ϕ_0 in the frictionless low-shear limit, and ϕ_m in the frictional high-shear limit. The exponent β is a fitting parameter that is generally taken to be ≈ 2.[18,20,35,36]

We identify ϕ_0 as the particle concentration at which the low-shear Newtonian viscosity (taken to be the minimum viscosity if shear thinning is present) diverges as a function of packing fraction. From graphs as in Fig. 3a, where we plot $\eta_r^{-1/\beta}$ as a function of ϕ, we can read off ϕ_0 as the intercept with the horizontal axis. Using $\beta = 2$ as the value that best linearized the data in such plot, this leads to $\phi_0(\mathrm{AR1}) = 55.7\%$. Upon increasing the aspect ratio of the particles eight-fold, this decreases to $\phi_0(\mathrm{AR8}) = 50.6\%$. Increasing aspect ratio further to 11 decreases ϕ_0 again by nearly 5 percentage points, to $\phi_0(\mathrm{AR11}) = 45.2\%$.

Similarly, we use Equation 1 to extract the frictional jamming packing fraction ϕ_m by considering the high-shear viscosity at the upper end of shear thickening (Fig. 3b), taking the maximum viscosity. In this case, $\beta = 1.8$ best linearized the data. For some of the highest packing fractions the suspensions were so easily driven into the shear jammed state that it was experimentally unclear if shear jamming, together with slip, occurred already just beyond the viscosity minimum (note that a solid-like, fully shear jammed state cannot be probed reliably with a steady-state viscosity measurement[20,37]). Therefore, to obtain ϕ_m via extrapolation we only use data for $\phi(\mathrm{AR1}) < 45.3\%$, $\phi(\mathrm{AR8}) < 38.0\%$, and $\phi(\mathrm{AR11}) < 32.0\%$.

As the aspect ratio Γ increases from 1 to 8 to 11, ϕ_m is found to decrease from 48.8% to 38.6% to 32.8%, respectively. This large reduction by 16 percentage points in ϕ_m from changing particle anisotropy stands in stark contrast to the small, $\sim$1% shift in ϕ_m observed when the effective, hydrogen-bonding-induced interparticle friction was changed by a factor 2.[21]

For random packings of sedimented rods a similar lowering of the packing fraction with increasing aspect ratio has been observed and associated with a concomitant increase in the number of rod-rod contacts.[22] It thus appears from our results that even under shear, were one would expect alignment, the remaining randomness in the rod orientations is sufficient to depress the packing fraction values for the onset of frictionless (ϕ_0) as well as frictional (ϕ_m) jamming.

The packing fraction range over which shear jamming is observable is given by the interval from ϕ_m to ϕ_0 (assuming the necessary shear stress is achievable). Figure 3c shows that this range nearly doubles as the aspect ratio Γ is increased from 1 to 8. We interpret that as an indication of how effective frictional interactions can be in enhancing the mechanical stability of the network formed by rods that are sheared into contact. A further increase in Γ from 8 to 11 delivers only a very modest enhancement of $\phi_0 - \phi_m$. While longer rods will lead to more contacts at low shear and thus, as observed, to jamming at smaller ϕ_0, we speculate that this does not also enhance the range $\phi_0 - \phi_m$ further because of the competing effect of better alignment at large shear.

To show these changes with aspect ratio more directly, we con-

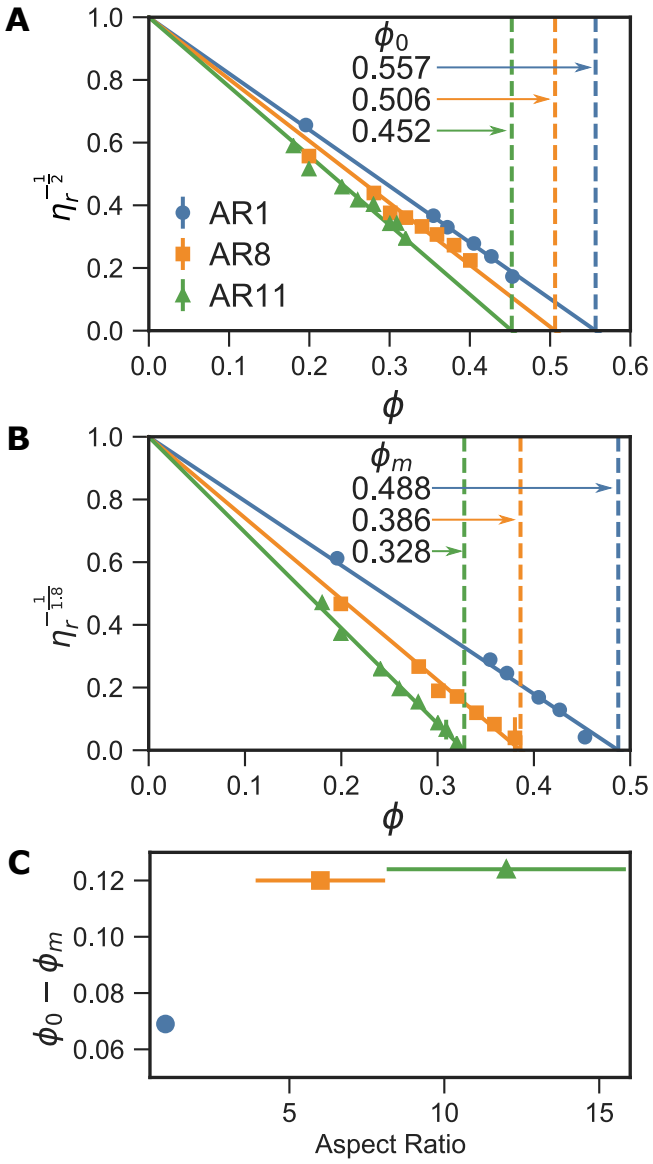

Fig. 3 A. Rescaled minimum low-shear viscosities as a function of packing fraction, enabling the determination of the frictionless jamming point ϕ_0 from linear least squares analysis. B. Rescaled maximum high-shear viscosities as a function of packing fraction, enabling the determination of the frictional jamming point ϕ_m from linear least squares analysis. In both A and B the exponent β was chosen to optimize the fit for all three curves. C. Dependence of the shear jamming packing fraction range, $\phi_0 - \phi_m$, on particle aspect ratio.

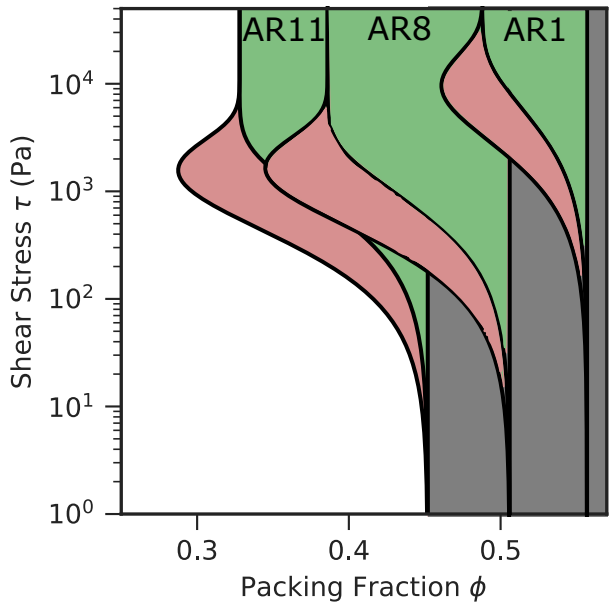

Fig. 4 State diagrams generated using the Wyart-Cates model for the AR11, AR8, and AR1 systems, showing regions that exhibit DST (red), shear jamming (green), or jammed-at-rest (gray) behavior.

struct state diagrams that delineate the regimes for discontinuous shear thickening (DST) and shear jamming (SJ) as a function of packing fraction ϕ and applied shear stress τ. We base these diagrams on the model by Wyart and Cates,[17] assuming infinitely hard particles and taking as input parameters the values of ϕ_m and ϕ_0, obtained from Fig. 3, as well as the characteristic stress τ^* at which the lubrication layers between particles break down and frictional interactions switch on. This stress value is obtained by quantitatively matching flow curves predicted by the Wyart-Cates model with data from Fig. 2, as was done in Ref. [21]. A more detailed description of the process to generate these state diagrams can be found in the Supplementary Information.

In these state diagrams, shown in Figure 4, ϕ_0 is the left boundary of the regime (grey) where jamming occurs in the absence of shear simply by increasing particle density, while ϕ_m is the leftmost boundary of the SJ regime (green). The DST regime is indicated by the red color.

In many suspensions of spherical particles that exhibit pronounced DST, an SJ regime is not readily observed.[21] This is either because the frictional interactions are weak, so that ϕ_m is extremely close to ϕ_0 and it becomes difficult to prepare a suspension that is not already jammed a rest, or because τ^* is so large that the stress required for SJ at any concentration $\phi < \phi_0$ becomes prohibitive. As Fig. 4 shows, the frictional interactions produced via the hydrogen bonding particle surfaces in this work, by contrast, generate a wide packing fraction interval for SJ already at aspect ratio Γ=1. Referring back to the flow curves in Figure 2 we note that, beyond increasing the effective friction via short-range, stress-dependent hydrogen bonding, this surface functionalization in our solvent does not introduce significant longer-ranged attractive forces, which would have led to the large yield stresses and a pronounced shear thinning regime such as that seen by others.[32,38]

The state diagrams highlight that increasing Γ not only shifts ϕ_0 and ϕ_m to lower values and enlarges the packing fraction range for DST and SJ, but also lowers the shear stress required to enter the DST and SJ regimes by almost a factor of 10. Since all particles have the same surface functional groups, this clearly demonstrates the independent role of the aspect ratio and the possibilities this opens up to control the location and extent of the SJ regimes as a function of ϕ and τ. In fact, compared to tuning the frictional interactions for fixed spherical shape,[21] the effect achievable by changing the aspect ratio Γ is strikingly large. Interestingly, most of this effect occurs up to Γ=8, while further increase of the aspect ratio does not appear to reduce the onset stress for SJ in any significant way and simply shifts the $[\phi_m, \phi_0]$ interval to lower values.

These findings provide an important experimental baseline for extending current models and simulations of dense suspension shear jamming to anisotropic particle shapes. They also provide new opportunities to design and optimize stress-adaptive materials. In such applications, it can be advantageous to obtain pronounced shear thickening and reversible, jamming-induced solidification with only a small amount of added particles. As Fig. 4 shows, with Γ=11 this can be achieved at particle concentrations as low as ϕ of 30% and 33%, respectively.

Conflicts of Interest

There are no conflicts to declare.

Acknowledgements

The authors thank Daniel Blair for helpful discussions regarding the particle synthesis, and Endao Han and Abhinendra Singh for helpful discussions. This work was supported by the Army Research Office through Grant W911NF-16-1-0078, and by the Chicago Materials Research Center/MRSEC, which is funded by the National Science Foundation through Grant NSF-DMR 1420709. HX and MG thank the Heising-Simons Foundation for support.

References

1 E. Brown and H. M. Jaeger, *Phys. Rev. Lett.*, 2009, **103**, 086001.
2 I. R. Peters, S. Majumdar and H. M. Jaeger, *Nature*, 2016, **532**, 214–217.
3 R. Hoffman, *Trans. Soc. Rheol.*, 1972, **166**, 155–173.
4 H. Barnes, *J. Rheol.*, 1989, **33**, 329–366.
5 J. Bender and N. J. Wagner, *The Journal of Chemical Physics*, 1996, **40**, 899–916.
6 B. J. Maranzano and N. J. Wagner, *Journal of Rheology*, 2001, **45**, 1205–1222.
7 N. J. Wagner and J. F. Brady, *Physics Today*, 2009, **62**, 27–32.
8 N. Fernandez, R. Mani, D. Rinaldi, D. Kadau, M. Mosquet, H. Lombois-Burger, J. Cayer-Barrioz, H. J. Herrmann, N. D. Spencer and L. Isa, *Phys. Rev. Lett.*, 2013, **111**, 108301.
9 N. Y. C. Lin, B. M. Guy, M. Hermes, C. Ness, J. Sun, W. C. K. Poon and I. Cohen, *Physical Review Letters*, 2015, **115**, 228304.

10 J. R. Royer, D. L. Blair and S. D. Hudson, *Physical Review Letters*, 2016, **116**, 188301.

11 R. Mari, R. Seto, J. F. Morris and M. M. Denn, *J. Rheol.*, 2014, **58**, 1693–1724.

12 A. Singh, R. Mari, M. M. Denn and J. F. Morris, *J. Rheol.*, 2018, **62**, 457–468.

13 R. Seto, R. Mari, M. F. Jeffrey and M. M. Denn, *Phys. Rev. Lett.*, 2013, **111**, 218301.

14 P. Kumar, D. Gold, D. L. Blair, A. Baskaran and J. S. Urbach, *Soft Matter*, 2014, **10**, 6514–6519.

15 B. Liu, M. Shelley and J. Zhang, *Physical Review Letters*, 2010, **105**, 188301.

16 S. R. Waitukaitis and H. M. Jaeger, *Nature*, 2012, **487**, 205–9.

17 M. Wyart and M. E. Cates, *Phys. Rev. Lett.*, 2014, **112**, 098302.

18 A. Singh, R. Mari, M. M. Denn and J. F. Morris, *Journal of Rheology*, 2018, **62**, 405.

19 J. F. Morris, *Physical Review Fluids*, 2018, **3**, 110508.

20 E. Han, N. M. James and H. M. Jaeger, *arXiv:1810.11887v1*, 2018.

21 N. M. James, E. Han, R. A. Lopez De La Cruz, J. Jureller and H. M. Jaeger, *Nat. Mat.*, 2018, **17**, 965–970.

22 A. P. Philipse, *Langmuir*, 1996, **12**, 1127–1133.

23 S. Williams and A. Philipse, *Phys. Rev. E.*, 2003, **67**, 051301.

24 K. Desmond and S. V. Franklin, *Phys Rev E*, 2006, **73**, 031306.

25 S. Mueller, E. W. Llewellin and H. M. Mader, *Proceeds of the Royal Society A*, 2010, **466**, 1201–1228.

26 A. P. R. Eberle, D. G. Baird and P. Wapperom, *Industrial Engineering & Chemical Research*, 2008, **47**, 3470–3488.

27 R. Sahoo and S. Dhara, *Fluids*, 2018, **3**, 1–15.

28 P. Kahl and L. Noirez, *Liquid Crystals Reviews*, 2016, **4**, 135–151.

29 M. Solomon and P. Spicer, *Soft Matter*, 2010, **6**, 1391–1400.

30 R. G. Egres and N. J. Wagner, *Journal of Rheology*, 2005, **49**, 719–746.

31 E. Brown, H. Zhang, N. A. Forman, B. W. Maynor, D. E. Betts, J. M. DeSimone and H. M. Jaeger, *Phys. Rev. E.*, 2011, **84**, 031408.

32 Y. Ye, H. Xiao, K. Reaves, B. McCulloch, J. F. Mike and J. L. Lutkenhaus, *Appl. Nano Mater.*, 2018, **1**, 2774–2784.

33 A. Kuijk, A. van Blaaderen and A. Imhof, *J. Am. Chem. Soc.*, 2011, **133**, 2346–2349.

34 I. M. Krieger and T. J. Dougherty, *Trans. Soc. Rheol.*, 1959, **3**, 137–152.

35 S. Maron and P. Pierce, *J. Coll. Sci.*, 1956, **11**, 80–95.

36 D. Quemada, *Rheol. Acta.*, 1977, **16**, 82–94.

37 M. Hermes, B. M. Guy, W. C. K. Poon, G. Poy, M. E. Cates and M. Wyart, *Journal of Rheology*, 2016, **60**, 905–916.

38 R. P. Murphy, K. Hong and N. J. Wagner, *Langmuir*, 2016, **32**, 8424–8435.

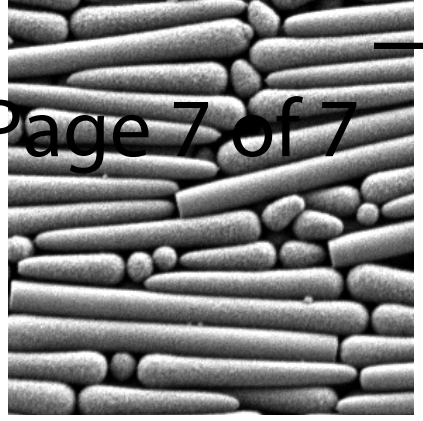

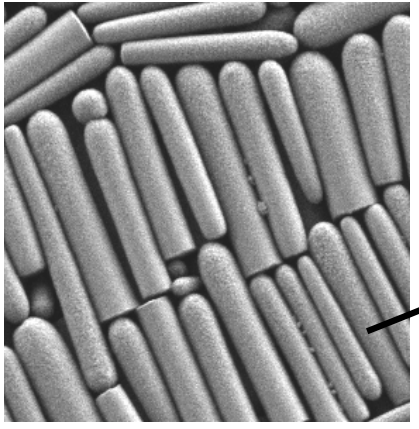

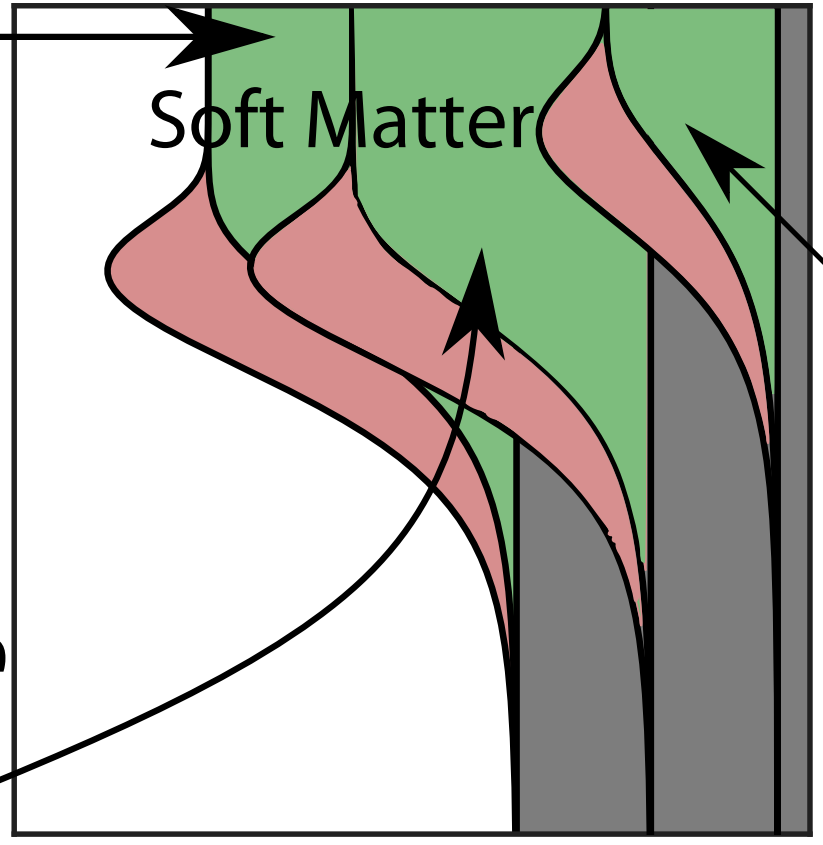
log shear stress
packing fraction